Enhanced spin relaxation in an ultrathin metal film by the Rashba-type surface

Nobuhiro Miyata,[1] Hisashi Narita,[2] Manami Ogawa,[2] Ayumi Harasawa,[2] Rei Hobara,[1] Toru Hirahara,[1] P. Moras,[3] D. Topwal,[4] C. Carbone,[3] Shuji Hasegawa,[1] and Iwao Matsuda[2,*]

[1]*School of Science, the University of Tokyo, 7-3-1 Hongo, Bunkyo-ku, Tokyo 113-0033, Japan*

[2]*The Institute for Solid State Physics, the University of Tokyo, 5-1-5 Kashiwanoha, Chiba 277-8581, Japan*

[3]*Istituto di Struttura della Materia, Consiglio Nazionale delle Ricerche, Trieste, Italy*

[4]*International Centre for Theoretical Physics (ICTP), Strada Costiera 11, I-34100 Trieste, Italy*

(Received 25 October 2010; revised manuscript received 28 March 2011; published 6 May 2011)

We measured the magnetoconductance of bare and $\sqrt{3} \times \sqrt{3}$-Bi/Ag-terminated ultrathin Ag(111) films by the micro-four-point probe method as a function of the applied magnetic field. The experimental curves were analyzed by introducing the results of photoemission investigation and band-structure calculations into the Hikami-Larkin-Nagaoka formula, in order to derive the characteristic fields of the two systems. The formation of the Rashba-type surface alloy was found to reduce the spin-relaxation time in the ultrathin film significantly.

DOI: 10.1103/PhysRevB.83.195305 PACS number(s): 73.63.Hs, 72.15.Rn, 79.60.−i, 72.25.Ba

I. INTRODUCTION

Achieving a detailed understanding of the spin-transport phenomena in thin metal films is one of the central topics of spintronics. Nowadays, research in this field focuses on the nanometer/subnanometer thickness regime, where intriguing spin-dependent functional behaviors can manifest due to the interaction of spin and charge degrees of freedom with the low-symmetry environment. In a thin film the size reduction along one axis down to a few atomic layers increases the surface/volume ratio and drives quantum-mechanical effects. In the thoroughly studied case of Ag films on Si(111),[1,2] for instance, quantum size effects manifest in the film electronic structure with the formation of discrete quantum-well states (QWS's), observable by photoemission spectroscopy at 1–8 nm thickness. Recent experimental reports indicate the possibility to tailor the spin and electronic configurations of the QWS's in Ag films on Si(111) by purposely perturbing the film/substrate or film/vacuum interfaces with foreign atomic species.[3–6] These results encourage further investigations with the aim of examining the link between electronic band structure and spin-dependent transport phenomena in the class of thin metal films.

In this paper we report on the magnetoconductance measurements performed on bare and $(\sqrt{3} \times \sqrt{3})$-Bi/Ag-covered ultrathin Ag(111) films by the micro-four-point probe (MFPP) method.[7,8] For both systems, we detect weak localization and weak antilocalization effects, with significantly different magnetic-field dependence in the two cases. The $(\sqrt{3} \times \sqrt{3})$-Bi/Ag (Rashba-type) surface[9,10] appears to reduce by almost one order of magnitude the spin-relaxation time of the electrons in the ultrathin metal film, without affecting the phase coherence time.

II. EXPERIMENT

Magnetotransport measurements in the present research were performed with our home-made multiprobe system which operates under ultrahigh vacuum conditions.[7] Figure 1(a) shows a schematic drawing of the measurement geometry of a MFPP (Ref. 8) and a sample. The magnetic field was applied along the normal to the sample surface. The outer and inner two probes of MFPP were used for the current flow and the voltage measurement ΔV, respectively. The Ag(111) film was prepared by deposition of 15 Ag monolayers (MLs) on a Si(111)-7×7 surface of a Si(111) wafer (n type, 1–10 Ω cm) at 150 K, followed by annealing at room temperature (the two-step growth procedure).[11] The $\sqrt{3} \times \sqrt{3}$-Bi/Ag phase was obtained by deposition of 1/3 ML Bi at 400 K on the film surface.[4,5] The crystalline quality of the samples was checked by reflection high-energy electron diffraction. The films are known to be atomically flat enough to form QWS's therein.[2,4–6] The magnetoconductance was measured by the MFPP method with a typical probe spacing of 20 μm at 7.6 K, to inhibit any probe-current flow through the Si substrate:[12,13] the carriers in the substrate were frozen out at this temperature.

III. RESULTS AND DISCUSSION

Solving the Poisson equation for the linear probe configuration with the equidistant probe-spacing, Fig. 1(a), the measured resistance $\frac{\Delta V}{I}$ is related with magnetoconductance σ as $\frac{\Delta V}{I} = \frac{\ln 2}{\pi}\frac{1}{\sigma} = \frac{\ln 2}{\pi} R_s(1 + \mu^2 B^2)$, where R_s and μ are sheet resistance and the mobility of the carriers, respectively.[14,15] The factor $\mu^2 B^2$ accounts for the classical magnetoresistance, which shows negligible effect at ordinary magnetic-flux densities, except for very high mobility samples. In the classic limit, μ equals $\frac{e\tau_0}{m^*}$, where τ_0 corresponds to relaxation time at zero magnetic field. Inserting typical effective mass (m^*) of the Ag QWS subbands and τ_0, determined by the present experiments (described below), one finds $\mu^2 B^2 \ll 1$ even at the maximum magnetic field ($B = 1$T) of the magnetoconductance measurement in Fig. 1(b).

Figure 1(b) shows the variation of the magnetoconductance, $\sigma(B) - \sigma(B = 0) = \Delta\sigma$, as a function of the applied magnetic field B, for the bare and $\sqrt{3} \times \sqrt{3}$-Bi/Ag-terminated 15-ML Ag(111) films. The magnetoconductance curves of both systems display signatures of weak antilocalization (decrease of $\Delta\sigma$) under weak magnetic field and weak localization effects (increase of $\Delta\sigma$) under strong magnetic field,[15] with a reversing field of 0.1 T for the bare Ag and about 0.4 T for the Bi-covered film. These two quantum interference effects are

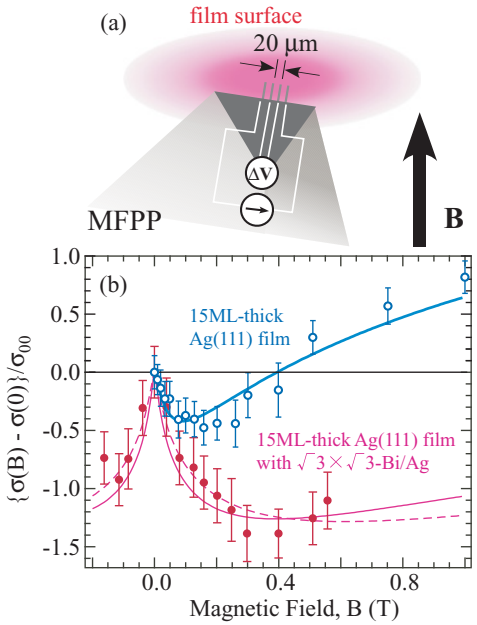

FIG. 1. (Color online) (a) Schematic drawing of the experimental geometry. Magnetic field is applied along the surface normal direction. The probe distance, adopted in the measurement, is indicated. (b) Magnetoconductance data for the bare (blue open circles) and $\sqrt{3}\times\sqrt{3}$- Bi/Ag-terminated (purple solid circles) 15-ML Ag(111) film with the measurement error bars. Solid and broken lines are fits to the data according to the Hikami-Larkin-Nagaoka (HLN) formula, Eq. (1). Two possible curve fits were performed for the Bi/Ag(111) film with the different fitting parameters. σ_{00} is the quantum unit of conductance.

quantitatively described by the Hikami, Larkin, and Nagaoka (HLN) formula using the four characteristic fields B_0, B_i, B_{so}, and B_s (the indices, 0, i, so, and s, stand for elastic, inelastic, spin-orbit, and spin-flip scattering, respectively):[15,16]

$$\Delta\sigma = \sigma(B)-\sigma(B=0) = -\sigma_{00}\left\{\Psi\left(\frac{1}{2}+\frac{B_1}{B}\right)+\ln\left(\frac{B}{B_1}\right) - \frac{3}{2}\left[\Psi\left(\frac{1}{2}+\frac{B_2}{B}\right)+\ln\left(\frac{B}{B_2}\right)\right] + \frac{1}{2}\left[\Psi\left(\frac{1}{2}+\frac{B_3}{B}\right)+\ln\left(\frac{B}{B_3}\right)\right]\right\}, \quad (1)$$

where $B_1 = B_0 + B_{so} + B_s$, $B_2 = B_i + \frac{4}{3}B_{so} + \frac{2}{3}B_s$, $B_3 = B_i + 2B_s$, Ψ is the digamma function, and $\sigma_{00} = \frac{e^2}{2\pi^2\hbar} = 1.2\times10^{-5}\,\Omega^{-1}$ is the quantum unit of conductance.

The HLN formula fits the experimental curves well, as shown in Fig. 1(b). In the fitting procedure we neglect magnetic scattering ($B_s = 0$) because of no magnetic impurity and assume that the elastic scattering is described by the Drude model, thus being independent from the external magnetic field ($B_0 = \text{const}$).[15] The free parameters in the fits remain, therefore B_i and B_{so}, which determine the strength of the weak localization and the weak antilocalization effects, respectively.

For a single free-electron band the characteristic fields are related to the carrier relaxation times (τ_p, $p = 0,i,so,s$) by $B_p = \frac{\hbar}{4eD\tau_p}$, where $D = \frac{1}{2}\tau_0 v_F^2$ is the diffusion constant and v_F is the Fermi velocity. More generally, for a given electronic structure this relation becomes[17,18]

$$B_p = \frac{e\hbar N^{\mathrm{DOS}}}{4\sigma_0\tau_p}, \quad (2)$$

where

$$N^{\mathrm{DOS}} = \sum_i \int dl_{k_{F//,i}} \frac{2}{(2\pi)^2}\frac{1}{|\hbar v_{F,i}|} \quad (3)$$

is the two-dimensional density of states at Fermi level (E_F), and $k_{F//,i}$ ($v_{F,i}$) is the Fermi wave vector (the Fermi velocity) of the ith QWS subband.

As evidently shown in Eq. (2), extraction of τ_p from B_p requires N^{DOS}, and thus a detailed knowledge of the electronic structure of the systems, Eq. (3). To evaluate N^{DOS}, we have taken the following steps: (i) Fermi surface and band mappings of the sample by angle-resolved photoemission spectroscopy, (ii) experimental extraction of Fermi wave vector $k_{F//}$, (iii) semiempirical evaluation of the Fermi velocity v_F by the two-dimensional (2D) nearly free electron model, and (iv) determination of N^{DOS} through summation of all the line integrals along the Fermi rings of the bands, Eq. (3).

A. Step (i): Photoemission Fermi surface and band mapping

The angle-resolved photoemission spectroscopy measurements were performed at the vacuum ultraviolet VUV-Photoemission (ELETTRA) and BL-18,19A (Photon Factory) beamlines.[4,5] Figures 2(a) and 2(b) show Fermi surfaces and Figs. 2(c) and 2(d) show band dispersion curves for (a), (c) the

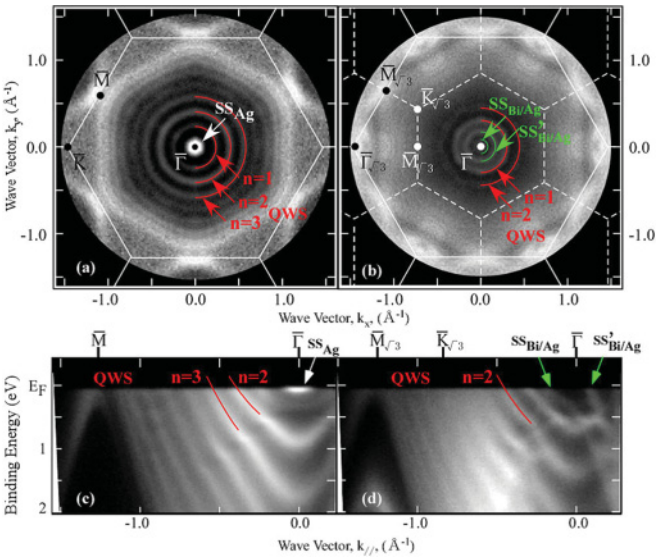

FIG. 2. (Color online) Top row: Photoemission Fermi surfaces for (a) bare and (b) $\sqrt{3}\times\sqrt{3}$- Bi/Ag-terminated 15-ML Ag(111) films measured at $h\nu = 49.6$ eV. The 1×1 and $\sqrt{3}\times\sqrt{3}$ surface Brillouin zones, along with their symmetry points, are also shown as solid and broken lines, respectively. Lines are used to mark the energy contours of QWS's and SS's. Bottom row: Gray-scale band diagrams measured along the $\overline{\Gamma}$-$\overline{\mathrm{M}}$ surface axis of the (c) bare and (d) Bi-covered Ag layer. Red solid lines are obtained from parabolic fits from parabolic fits of band dispersion near the Fermi level (E_F).

bare and (b), (d) the $\sqrt{3} \times \sqrt{3}$-Bi/Ag-covered 15-ML Ag(111) films. All circular and hexagonal-like Fermi energy contours in Fig. 2(a) are QWS subbands, except for the spot at $\overline{\Gamma}$, which is the Ag(111) surface state (SS).[19] These QWS's have free-electron-like in-plane dispersion [Fig. 2(c)], except in the proximity of the surface-projected bulk band edges of Si.[2] The electronic structure of the $\sqrt{3} \times \sqrt{3}$-Bi/Ag(111) film [Fig. 2(d)], instead, appears to be more complex, due to several surface bands, spin-split by the Rashba interaction, which disperse downward from the $\overline{\Gamma}$ point.[4–6] The energy shift of the QWS subbands toward higher binding energies further reflects the Bi/Ag alloy formation, which determines the electron confinement condition at the vacuum/film interface.[1] Notably, for the Bi-terminated film SS's and QWS's give rise to hybrid states at specific (spin- and symmetry-selected) band crossings only below E_F.[4,5] This fact may simplify the interpretation of our transport measurements: from the electronic structure point of view, one may approximate the film and the surface as independent layers in the proximity of E_F.

In our layer model, consisting of surface and film layers, the total B_p is expressed in terms of the partial B_p's as[17,18]

$$B_p/R = B_{p,\mathrm{film}}/R_{\mathrm{films}} + B_{p,\mathrm{surface}}/R_{\mathrm{surface}}, \qquad (4)$$

where R is total resistance, while R_{surface} and R_{film} are the resistances of the individual layers. The $B_{p,j}/R_j$ value is proportional to the density of states and thickness of the jth layer.[18] Surface and film thickness are easily defined. N^{DOS}, instead, must be obtained from the v_F and $k_{F//}$ values derived from the measured band structures (Fig. 2).

B. Step (ii): Experimental extraction of $k_{F//}$

Figure 3(a) displays momentum distribution curves of the photoemission signal at E_F. The largest photoemission peak for the Ag(111) film (top line) originates from the SS band[19] and has $k_{F//} = 0.13$ Å^{-1}. Other peaks correspond to some bands of the QWS's expected to cross E_F. In the present experimental conditions we can distinguish only the $n = 1{-}5$ states, while the remaining states merge into a broad spectral feature. Concerning the Bi/Ag(111) film (bottom line), the photoemission peaks of the $\sqrt{3} \times \sqrt{3}$-Bi/Ag SS's[4,5] are observed around the original and back folded $\overline{\Gamma}$ points (this second type of points is labeled with $\overline{\Gamma}_{\sqrt{3}}$). Due to the features introduced by the $\sqrt{3} \times \sqrt{3}$ periodicity, only the $n = 1,2$ QWS's subbands could be clearly identified at slightly larger $k_{F//}$ values with respect to the corresponding states of the bare Ag.

C. Step (iii): Semiempirical v_F evaluation by the 2D NFE simulation

In order to infer the $k_{F//}$ and v_F values over the whole two-dimensional surface Brillouin zone from the limited experimental information, we have performed electronic structure simulation with the 2D nearly free electron (NFE) model. Figure 3(b) displays the experimental v_F values (diamonds and squares, corresponding to data points measured along $\overline{\Gamma} - \overline{\mathrm{M}}$ and $\overline{\Gamma} - \overline{\mathrm{K}}$, respectively) as a function of $k_{F//}$, as determined from the gradient of the dispersion curves [Figs. 2(c) and 2(d) show some of them as continuous lines]. The calculated v_F's (thick lines) reproduce well the experimental points both near $\overline{\Gamma}$ (effective mass $m* = 0.85$ in units of the electron rest mass), where also the free electron model (thin lines) matches satisfactorily with the data, and close to the zone boundaries (in this region the free electron model fails), with a band intermixing energy of 1 eV. With these band parameters, the NFE dispersion curves can be determined for the whole two-dimensional surface Brillouin zone.

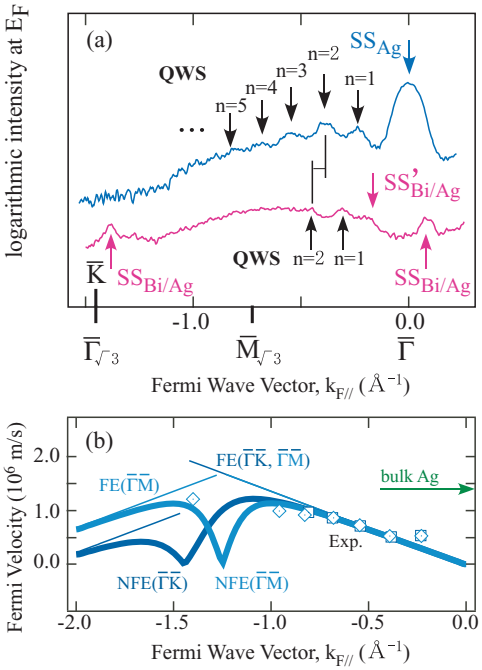

FIG. 3. (Color online) (a) Momentum distribution curves in logarithmic scale of the photoemission intensity at E_F for the bare (top curve) and $\sqrt{3} \times \sqrt{3}$-Bi/Ag-terminated (bottom curve) 15-ML Ag(111) film. (b) Comparison between the v_F values obtained from the photoemission data (symbols) and the band-structure calculation using the NFE (thick lines, $m^*/m_0 = 0.85$, off-diagonal element 1.0 eV) and the free electron (thin lines, $v_F = \hbar k_{F//}/m^*$, $m^*/m_0 = 0.85$) models. Diamonds and squares refer to data taken along $\overline{\Gamma} - \overline{\mathrm{M}}$ and $\overline{\Gamma} - \overline{\mathrm{K}}$, respectively.

D. Step (iv): Evaluation of N^{DOS}

Through the calculation of Eq. (3) with our optimized 2D NFE model, N^{DOS} for Ag(111) and Bi/Ag(111) film layers has the same value (3×10^{38} m^{-2} J^{-1}), due to the significant contribution from the bunch of the outer hexagonal-like contours characterizing both Fermi surfaces (Fig. 2). For the surface layer, instead, different values are obtained. For the Ag(111) SS_{Ag} band,[19] $v_F = 3 \times 10^5$ ms^{-1} at $k_F = 0.13$ Å^{-1} and $N^{\mathrm{DOS}} = 1 \times 10^{37}$ m^{-2} J^{-1}. For the two SS bands, $SS_{Bi/Ag}$ and $SS'_{Bi/Ag}$, of the $\sqrt{3} \times \sqrt{3}$-Bi/Ag(111) system, $v_F = 8 \times 10^5$ ms^{-1} ($k_F \sim 0.1$ Å^{-1}) and 1.7×10^6 ms^{-1} ($k_F \sim 0.2$ Å^{-1}), respectively. In total, $N^{\mathrm{DOS}} = 4 \times 10^{36}$ m^{-2} J^{-1} for the Bi/Ag film. Since an electronic state of the surface state, in general, extends over 1–2 layers, the thickness ratio between the surface layer and the film is estimated $1/14 \sim 2/14$. Then, the $B_{p,\mathrm{surface}}/R_{\mathrm{surface}}$ value is less than 0.5% of $B_{p,\mathrm{film}}/R_{\mathrm{film}}$

TABLE I. A summary of relaxation time and mean free path of various scattering schemes in 15-ML-Ag(111) films with the bare and the $\sqrt{3} \times \sqrt{3}$-Bi-covered surfaces.

	Bare Ag(111)	$\sqrt{3} \times \sqrt{3}$-Bi/Ag
Scattering	relaxation time (mean free path)	relaxation time (mean free path)
Elastic	$\tau_0 \sim 1 \times 10^{-15}$ s (nanometer scale)	$\tau_0 \sim 1 \times 10^{-15}$ s (nanometer scale)
Inelastic	$\tau_i \sim 3 \times 10^{-11}$ s (10-μm scale)	$\tau_i \sim 5 \times 10^{-11}$ s (10-μm scale)
Spin orbit	$\tau_{so} \sim 6 \times 10^{-12}$ s (1–10-μm scale)	$\tau_{so} \leqslant 1 \times 10^{-12}$ s (100 nm–1-μm scale)

and the measured magnetoconductance change in Fig. 2 corresponds to a good approximation to that of the film only, $B_p/R \approx B_{p,\mathrm{film}}/R_{\mathrm{film}}$.

E. Individual relaxation time, τ_p

Introducing the calculated N^{DOS} of the film and experimental B_p values into Eq. (2), the relaxation times are determined. The elastic scattering time τ_0 can be estimated by using the Drude formula. The measured resistance $\frac{\Delta V}{I}$ at $B = 0$ T of a 15-ML Ag(111) film, covered with either a clean Ag(111) surface or the $\sqrt{3} \times \sqrt{3}$-Bi/Ag surface, was 18 Ω and $\tau_0 \sim 1 \times 10^{-15}$ s.

The HLN fitting curve of the clean Ag(111) film in Fig. 2 gives $\tau_i = 3 \times 10^{-11}$ s and $\tau_{so} = 6 \times 10^{-12}$ s. On the other hand, the possible fitting curves of the $\sqrt{3} \times \sqrt{3}$-Bi-covered Ag(111) film provide $\tau_i = 4 - 6 \times 10^{-11}$ s and $\tau_{so} = 0.9 - 1 \times 10^{-12}$ s. Notably the choice of τ_0 does not affect the estimation of τ_i and τ_{so}. These results clearly show that, by changing the surface atomic layers, τ_{so} has reduced by about one order of magnitude (∼85%), indicating a significant increase of spin relaxation in the metal film. On the other hand, the precise evaluation of τ_i has remained uncertain due to a lack of magnetotransport data at $B > 0.6$ T. Within the experimental resolution, τ_i is likely similar between the bare and $\sqrt{3} \times \sqrt{3}$-Bi-covered Ag(111) films. The electron mean free path in the Ag(111) film was calculated as a product of τ_p and $v_F \sim 10^6$ m/s, as estimated in Fig. 3(b). A summary of the relaxation time and the mean free path is listed in Table I. The elastic mean free path, corresponding to the momentum relaxation length, was evaluated to be nanometers while the inelastic (phase coherence) and spin-orbit (spin relaxation) lengths ranged 10 μm scale and submicron-10 μm scale, respectively.

The relaxation time scale of $10^{-12} \sim 10^{-11}$ s for τ_{so} and τ_i is quite consistent with the previous magnetotransport research for 2–6-ML-thick ultrathin Ag(111) films on the Si(111)7×7 substrate, prepared by the same process.[15] The relaxation time of the present results was longer, which is likely due to the distinctive growth morphology of Ag below and above the 6 MLs. The two-step growth procedure has been known to associate the magic thickness of 6 MLs: atomically flat Ag(111) film grows above 6 MLs and the multilayer Ag films are formed below 6 MLs.[11] Therefore difference of the relaxation time is likely understood in terms of the Ag film quality.

The present results have shown that spin-orbit scattering time decreases significantly, compared with the other relaxation time, when the surface of the ultrathin metal film changes. The spin-relaxation time (spin-orbit scattering probability) in metals has been generally modeled by the Elliot-Yafet model and it has been argued with the momentum relaxation time (momentum scattering probability).[20] In materials with small spin-orbit interaction, two relaxation times are proportional to each other and the ratio depends on the scattering scheme, i.e., scattering of impurities, boundaries, or phonons. Since, as listed in Table I, the momentum relaxation length of nanometers corresponds to the film thickness, a relation of scattering time between momentum relaxation and spin-orbit interaction at the surface is of interest. However, the $\sqrt{3} \times \sqrt{3}$-Bi/Ag-terminated Ag(111) film consists of the Rashba-type surface of the heavy element (Bi) and the spin-orbit interaction is so large that the proportional relation does not hold.[20] The complete understanding of these results requires more advanced spin transport theory and the present transport data are expected to help the development.

It has recently been reported that, in a Ag thin film, the spin flip probability at a surface scattering is the highest among the other mechanisms, impurity and phonon scatterings.[21] Regulation of the surface is thus the most efficient to control spin transport in a thin metal film. In contrast to doping of heavy atoms inside the film, the formation of the ordered surface alloy with the large spin-orbit interaction was demonstrated to induce the significantly large spin relaxation, while keeping the electrical conduction (mean free path) in the film.

IV. CONCLUSION

In summary, we measured the magnetoconductance of ultrathin Ag(111) films with two types of surface terminations by the MFPP method. The Rashba-type $\sqrt{3} \times \sqrt{3}$-Bi/Ag surface alloy markedly reduces the spin scattering time in the underlying layer with respect to the case of a bare Ag film. The decrease occurs without changes in the elastic-scattering and phase coherence time. Proper theoretical investigations are requested to understand in detail this mechanism.

ACKNOWLEDGMENTS

This work was supported by JSPS (KAKENHI 18360018) and Executive Program of Cooperation in the Fields of Science & Technology between the Government of Italy and the Government of Japan for the period from 2008 to 2009.

*imatsuda@issp.u-tokyo.ac.jp

[1] T.-C. Chiang, Surf. Sci. Rep. **39**, 181 (2000).

[2] I. Matsuda, T. Ohta, and H. W. Yeom, Phys. Rev. B **65**, 085327 (2002).

[3]T. Okuda, Y. Takeichi, K. He, A. Harasawa, A. Kakizaki, and I. Matsuda, Phys. Rev. B **80**, 113409 (2009).
[4]K. He, T. Hirahara, T. Okuda, S. Hasegawa, A. Kakizaki, and I. Matsuda, Phys. Rev. Lett. **101**, 107604 (2008).
[5]K. He, Y. Takeichi, M. Ogawa, T. Okuda, P. Moras, D. Topwal, A. Harasawa, T. Hirahara, C. Carbone, A. Kakizaki, and I. Matsuda, Phys. Rev. Lett. **104**, 156805 (2010).
[6]E. Frantzeskakis, S. Pons, H. Mirhosseini, J. Henk, C. R. Ast, and M. Grioni, Phys. Rev. Lett. **101**, 196805 (2008).
[7]N. Miyata, R. Hobara, T. Hirahara, S. Hasegawa, H. Narita, and I. Matsuda, Jpn. J. Appl. Phys. **50**, 036602 (2011).
[8]T. Tanikawa, I. Matsuda, R. Hobara, and S. Hasegawa, J. Surf. Sci. Nanotech. **1**, 50 (2003).
[9]C. R. Ast, J. Henk, A. Ernst, L. Moreschini, M. C. Falub, D. Pacilé, P. Bruno, K. Kern, and M. Grioni, Phys. Rev. Lett. **98**, 186807 (2007).
[10]F. Meier, H. Dil, J. Lobo-Checa, L. Patthey, and J. Osterwalder, Phys. Rev. B **77**, 165431 (2008).
[11]L. Huang, S. J. Chey, and J. H. Weaver, Surf. Sci. **416**, L1101 (1998).
[12]I. Matsuda and S. Hasegawa, J. Phys.: Condens. Matter **19**, 355007 (2007).
[13]I. Matsuda, C. Liu, T. Hirahara, M. Ueno, T. Tanikawa, T. Kanagawa, R. Hobara, S. Yamazaki, S. Hasegawa, and K. Kobayashi, Phys. Rev. Lett. **99**, 146805 (2007).
[14]D. H. Petersen, O. Hansen, R. Lin, and P. F. Nielsen, J. Appl. Phys. **104**, 013710 (2008).
[15]M. Henzler, T. Lċuer, and J. Heitmann, Phys. Rev. B **59**, 2383 (1999).
[16]S. Hikami, A. I. Larkin, and Y. Nagaoka, Prog. Theor. Phys. **63**, 707 (1980).
[17]H. Beckmann, T. Fulmer, D. Garrett, M. Hossain, and G. Bergmann, Phys. Rev. B **59**, 7724 (1999).
[18]G. Bergmann, Phys. Rev. Lett. **53**, 1100 (1984).
[19]S. Hüfner, *Photoelectron Spectroscopy: Principles and Applications* (Springer-Verlag, Berlin, 1996).
[20]I. Zutic, J. Fabian, and S. D. Sarma, Rev. Mod. Phys. **76**, 323 (2004).
[21]G. Mihajlović, J. E. Pearson, S. D. Bader, and A. Hoffmann, Phys. Rev. Lett. **104**, 237202 (2010).